Monthly Notices of the ROYAL ASTRONOMICAL SOCIETY

MNRAS **521,** 2806–2813 (2023) https://doi.org/10.1093/mnras/stad649
Advance Access publication 2023 March 2

The 2019 outburst of AMXP SAX J1808.4–3658 and radio follow up of MAXI J0911–655 and XTE J1701–462

K. V. S. Gasealahwe [1,2★] I. M. Monageng [1,2★] R. P. Fender,[1,3] P. A. Woudt [1] S. E. Motta [3,4] J. van den Eijnden,[3] D. R. A. Williams [5] I. Heywood,[3,6,7] S. Bloemen,[8] P. J. Groot,[1,2,8] P. Vreeswijk,[8] V. McBride,[1,2,9] M. Klein-Wolt,[8] E. Körding,[8] R. Le Poole,[10] D. Pieterse[8] and S. de Wet[1]

[1]*Department of Astronomy, University of Cape Town, Private Bag X3, Rondebosch 7701, South Africa*
[2]*South African Astronomical Observatory, P.O. Box 9, Observatory, 7935, South Africa*
[3]*Department of Physics, University of Oxford, Denys Wilkinson Building, Keble Road, Oxford OX1 3RH, UK*
[4]*Istituto Nazionale di Astrofisica, Osservatorio Astronomico di Brera, via E. Bianchi 46, I-23807 Merate (LC), Italy*
[5]*Jodrell Bank Centre for Astrophysics, School of Physics and Astronomy, The University of Manchester, Manchester M13 9PL, UK*
[6]*Department of Physics and Electronics, Rhodes University, PO Box 94, Makhanda 6140, South Africa*
[7]*South African Radio Astronomy Observatory, 2 Fir Street, Black River Park, Observatory, 7925, South Africa*
[8]*Department of Astrophysics/IMAPP, Radboud University, P.O. 9010, NL-6500 GL Nijmegen, the Netherlands*
[9]*IAU Office of Astronomy for Development, P.O. Box 9, Observatory, 7935, South Africa*
[10]*Leiden Observatory, Leiden University, P.O. Box 9513, NL-2300 RA Leiden, the Netherlands*

Accepted 2023 February 24. Received 2023 February 24; in original form 2022 July 21

ABSTRACT

We present radio coverage of the 2019 outburst of the accreting millisecond X-ray pulsar (AMXP) SAX J1808.4–3658, obtained with MeerKAT. We compare these data to contemporaneous X-ray and optical measurements in order to investigate the coupling between accretion and jet formation in this system, while the optical light curve provides greater detail of the outburst. The reflaring activity following the main outburst peak was associated with a radio re-brightening, indicating a strengthening of the jet in this phase of the outburst. We place quasi-simultaneous radio and X-ray measurements on the global radio:X-ray plane for X-ray binaries, and show they reside in the same region of luminosity space as previous outburst measurements, but significantly refine the correlation for this source. We also present upper limits on the radio emission from the AMXP MAXI J0911–655 and the transitional Z/Atoll-type transient XTE J1701–462. In the latter source, we also confirm that nearby large-scale structures reported in previous radio observations of the source are persistent over a period of ∼15 yr, and so are almost certainly background radio galaxies and not associated with the X-ray transient.

Key words: radio continuum: transients – X-rays: binaries.

1 INTRODUCTION

Neutron star (NS) X-ray binaries (XRBs) are binary systems comprising a NS that accretes matter from a companion star. A subgroup of these are systems with low-mass ($M_{\rm companion} < 1$ M$_\odot$) companions, and are thought to be considerably older than systems with a higher mass ($M_{\rm companion} \gtrsim 8$ M$_\odot$; Joss, Avni & Rappaport 1978). In a subset of the low-mass systems, the NS is observed to spin at periods significantly smaller than a second, either through the detection of pulsations in their X-ray flux or oscillations during thermonuclear Type I X-ray bursts on their surface (Patruno & Watts 2021). In accreting millisecond X-ray pulsars (AMXPs), of which SAX J1808.4–3658 (Wijnands & van der Klis 1998) is the prototype, the accretion and millisecond combination may be explained by the scenario of recycled pulsars. In this scenario the pulsar originates as a 'normal' pulsar that eventually spins down on a time-scale of $t \approx 10^6$ yr, possibly in combination with magnetic field decay. The pulsar is spun-up again through an accretion phase and manifests as an AMXP (Alpar et al. 1982; Backer et al. 1982; Srinivasan 2010) which emits pulsed X-rays with a period of 1–10 ms. Some pulsars are estimated to have a relatively low magnetic field strength of $\sim 10^8$ G. Two other empirical classifications of NS-XRBs at high accretion rate and low magnetic field ($\leq 10^9$ G) systems are known: the Atoll and Z sources. The former may also exhibit pulsations. These two classes are distinctly classified according to the ratio of their X-ray soft and hard energy bands often referred to as X-ray colours, traced over different time-scales (Hasinger & van der Klis 1989). For the Z sources, the hard and soft colours plotted against each other reveal a 'Z-shape' pattern traversed on time-scales of hours to days, while Atoll sources show a 'C-shape' pattern generally accompanied by an 'island' at large hard colours on time-scales ranging from weeks to months (Muno, Remillard & Chakrabarty 2002). Some sources display a blend of properties of the two classes as well as properties that enter in neither (e.g. Cir X-1; Moin et al. 2011). Most dramatically the NS transient XTE J1701–462 demonstrated a clear transition from Z-like to Atoll-like properties as its luminosity dropped resulting from a high mass transfer rate ($\dot{m}$) to a lower $\dot{m}$ during the outburst decay. This allowed to connect the two classes to accretion rate (Homan et al. 2007). This blurring

★ E-mail: kelebogile@saao.ac.za (KG); itu@saao.ac.za (IM)

of some Atoll and Z sources coupled with properties of AMXPs makes the distinction of the different classes of NS-XRBs poorly understood.

Interesting in their own right, accreting low-magnetic field NSs in the Z/Atoll/AMXP classes play a crucial role as a control sample to the black hole (BH) population in the context of the coupling between accretion and jet formation in BHs, which have no surface. While detailed studies of individual sources are important, a key global diagnostic of this jet:outflow (where the radio is from the jets and X-rays are observed from accretion flow) coupling is the use of the radio:X-ray luminosity plane (Gallo, Fender & Pooley 2003). One key result from such global studies is that the sample of black holes are typically more radio-loud (exhibiting brighter radio luminosities) than the populations of NSs for a given X-ray luminosity (Fender & Kuulkers 2001; Migliari & Fender 2006). Another key result is the slope of the radio:X-ray correlation. In BH systems in the hard X-ray state (or at relatively low luminosities) accretion is believed to be inefficient, as a large fraction of the gravitational potential energy is not radiated, but lost across the BH event horizon (Fender & Belloni 2012). In contrast, in NS systems accretion may be efficient as all the potential energy of the accreting matter is released at the NS surface. This may result in a steeper correlation (see e.g. discussion in Coriat et al. 2011). Multiple studies of NS systems, however, suggest that the slope of the correlation for some NS-XRBs is inconsistent with this assumption (Migliari & Fender 2006; Tudose et al. 2009; Deller et al. 2015; Gallo, Degenaar & van den Eijnden 2018). The correlation slope of some NSs being similar to that of BHs is surprising because the physical properties are different between the compact objects. In order to develop a better understanding of the radio:X-ray correlation for NS-XRBs, a quantitative analysis of luminosity strength is required of these systems. In this study, we do not consider high-magnetic field accreting NSs, which are less radio luminous and may well have a quite different flow geometry close to the NS, but we direct the interested reader to van den Eijnden et al. (2021) for details.

SAX J1808.4–3658 (SAX J1808 hereafter) is an XRB with an X-ray pulsation at 401 Hz. SAX J1808 was discovered in 1998 by the *Rossi X-ray Timing Explorer (RXTE*; Levine et al. 1996), and was the first confirmed AMXP (Wijnands & van der Klis 1998). SAX J1808 displays Type I thermonuclear X-ray bursts based on which a distance of 3.5 kpc was estimated (in't Zand et al. 1998; Galloway & Cumming 2006). An orbital period of ≈2 h (Chakrabarty & Morgan 1998) is known for the source. SAX J1808 is reported to go into semiregular outbursts with recurrence times between 2 and 4 yr. Previous outbursts from SAX J1808 were recorded in 1999, 2002, 2005, 2015 (Tudor et al. 2017). In this paper, we report on the 2019 outburst of SAX J1808 as observed with MeerKAT in radio (Williams et al. 2019). SAX J1808 was observed with the *X-ray telescope (XRT)* onboard the *Neil Gehrels Swift telescope* (*Swift*; Burrows et al. 2005) and the *Neutron Star Interior Composition ExploreR* (*NICER*; Gendreau, Arzoumanian & Okajima 2012) in the X-rays and additionally show the optical Las Cumbres Observatory (LCO) data reported in Baglio et al. (2020) to trace the main outburst via a multiwavelength approach, and to measure the radio:X-ray correlation for this outburst of the source.

Additionally, while we compare SAX J1808 to the rest of the AMXP radio and X-ray luminosity measurements ($L_R L_X$), we also report short MeerKAT observations of the AMXP MAXI J0911–655 (MAXI J0911, hereafter Homan et al. 2016; Serino et al. 2016) and transitional Atoll/Z-source XTE J1701–462 (XTE J1701, hereafter Homan et al. 2007).

2 OBSERVATIONS

2.1 MeerKAT observations

The 2019 outburst of SAX J1808 was monitored with MeerKAT at 1.28 GHz, through the ThunderKAT Large Survey Programme (Fender et al. 2016) and by *Swift* as part of an associate observing program. MeerKAT consists of 64 dishes and on average 61 dishes were available per observation. The outburst was monitored nearly weekly for six epochs (Table 1) from 2019 July 31 to 2019 August 31, for 15 min every week. J1939–6342 was observed for 5 min at the start of each observation, as the primary calibrator for flux and bandpass calibrations. The secondary calibrator, J1830–3602, was observed for 2 min before and after the target in each observation. All observations were performed with a total bandwidth of 860 MHz, divided into 4096 channels of width 209 kHz. The MeerKAT data were reduced using the semi-automated pipeline, OXKAT.[1] (Heywood 2020). The first generation process of OXKAT involves making use of CASA (McMullin et al. 2007) to perform averaging, flagging, and do cross- and self-calibration. Once the visibility and gain solution plots produced were satisfactory after inspection, the data were then flagged and imaged using the TRICOLOUR and WSCLEAN packages, respectively (Offringa et al. 2014). Thereafter, the second-generation processing was initiated to do self-calibration, plot gain solutions and a second output of images were produced. The flux densities were then determined using PYBDSF (Mohan & Rafferty 2015).

MAXI J0911 and XTE J1701 were observed with MeerKAT in the same way as SAX J1808. MAXI J0911 was observed around a phase of hard X-ray emission (Ng et al. 2021) on the 2021 July 8 and 26, while XTE J1701 was observed on the 2021 July 26 as part of a broader study of NS-XRBs with ThunderKAT. The sources were observed for 15 min for each observation and the reduction and analysis procedures are the same as those described above for SAX J1808, except the primary and secondary calibrator for MAXI J0911 were J0408−6545 and J0906−6829, respectively, and the secondary calibrator for XTE J1701 was J1744−5144.

2.2 X-ray observations

Swift/XRT provided a total of 21 observations of SAX J1808 of variable duration, of which 10 were between 2019 July 31 to 2019 August 31, taken quasi-simultaneously with MeerKAT. The overall *Swift/XRT* exposure time was formed by a number of snapshots, taken in both Windowed Timing (WT) mode and Photon Counting (PC) mode (Burrows et al. 2005), both providing data in the 0.3–10.0 keV energy band. Following the *XRT* reduction threads,[2] we extracted spectra from circular regions centred at the source position, with a radius of 30 pixels. When fitting the energy spectra we ignored data below 0.6 keV since spectra can be dominated by strong redistribution effects associated with the WT readout process, as well as trailing charge released from deep charge traps in the CCD on time-scales comparable to the WT readout time. The above might result in additional low energy events that may distort the spectrum. Spectra were then extracted following standard extraction procedures.[3]

Based on the radio observations taken of MAXI J0911 and XTE J1701, we followed up to check if any observations were taken with *Swift* at the time. The *Swift* Burst Alert Telescope survey data was found of both sources, which were within a day of quasi-simultaneity

[1]For more details, see https://github.com/IanHeywood/oxkat
[2]http://www.swift.ac.uk/analysis/xrt/#abs
[3]See https://www.swift.ac.uk/analysis/xrt/spectra.php

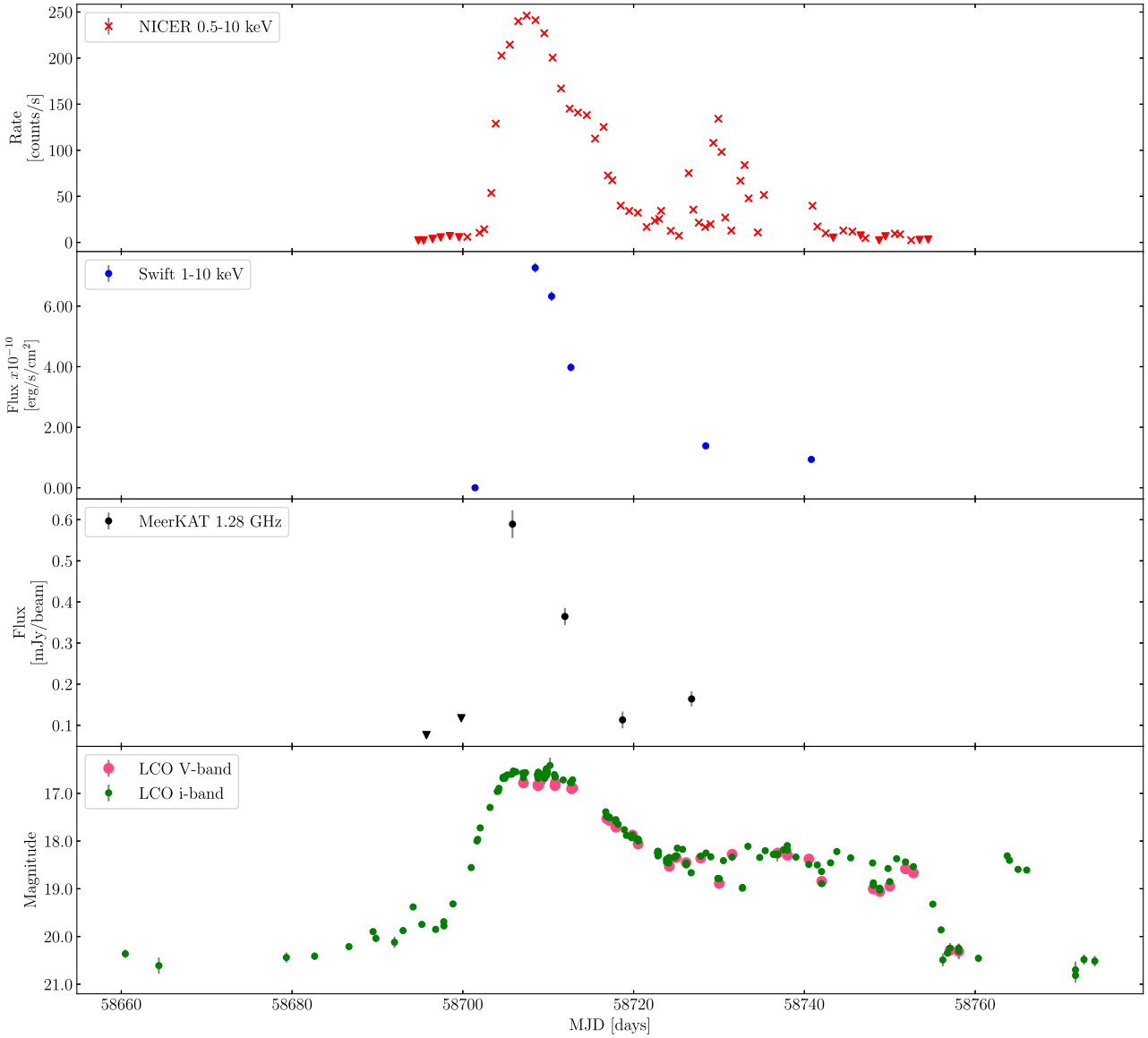

Figure 1. The 2019 outburst of SAX J1808 as seen in the X-ray (top panel: 0.5–10 keV, second panel: 1–10 keV), radio (third panel: 1.28 GHz), and optical (bottom panel: *V* and *i* band). The upper limits from *NICER* and the non-detections of the first two epochs in the radio are indicated with the red and black upside down triangles, respectively.

of the first epoch of MAXI J0911 radio observations and the single epoch of XTE J1701.

The *NICER* telescope observed the 2019 outburst of SAX J1808 extensively in X-rays, providing near-daily coverage of the outburst between 2019 July 30 and 2019 September 28 (Bult et al. 2019). In order to probe the overall evolution of the outburst, we analysed the cumulative data taken on each day, often combining a number of shorter exposures per MJD. We applied the FTOOL NICERL2 to perform the most recent calibration, after which we extracted the source count rate between 0.5 and 10 keV. To calculate the background count rate, we applied the *nicer_bkg_estimator* model, based on *RXTE* blank sky background fields (Jahoda et al. 2006), in the same energy band. During days where the source count rates does not exceed three times the background, we report 3σ upper limits. For the remaining observations, we show the light curve in the top panel of Fig. 1. Due to the small background rate compared to the source count rate during the majority of the outburst, for simplicity we plot the source count rates not background-corrected. Both the *Swift/XRT* and *NICER* spectra were fitted with a model in the form (tbfeo $*$ [continuum]), where tbfeo is an ISM model and *[continuum]* was either a powerlaw (POWER in XPEC), a disc-blackbody component (DISKBB), or a combination of disc-blackbody and a blackbody component (DISKBB + BBODYRAD). In modelling the interstellar absorption, we assumed abundances from Wilms, Allen & McCray (2000) and cross-sections from Verner et al. (1996). The *Swift/XRT* and *NICER* spectra were fitted in the 0.6–10 and 0.2–10 keV energy range, respectively. In both cases, we fixed the equivalent Hydrogen column density to $n_{\rm H} = 0.117 \times 10^{22}$ cm^{-2}.[4]

[4]See https://heasarc.gsfc.nasa.gov/cgi-bin/Tools/w3nh/w3nh.pl

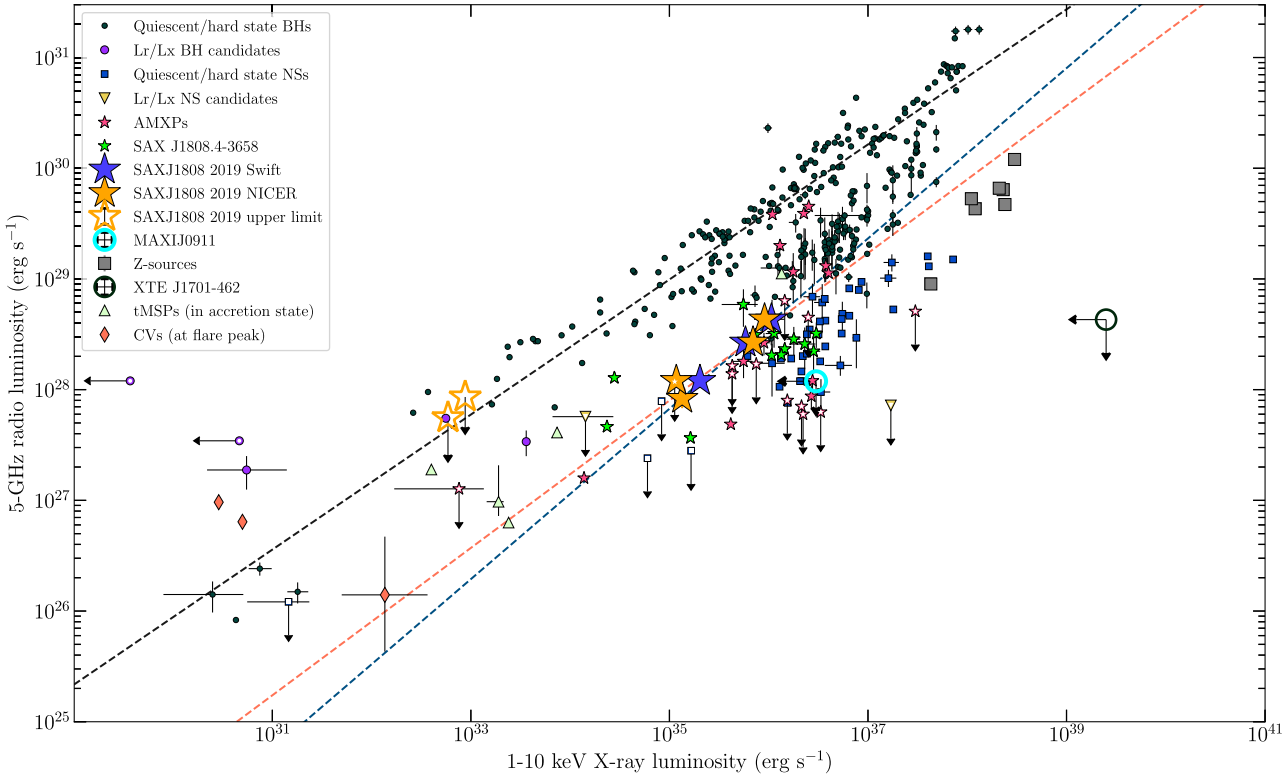

Figure 2. The radio:X-ray correlation for BH and NS sources labelled in terms of class (Migliari & Fender 2006; Bahramian et al. 2018), with previous SAX J1808 detections indicated with green stars and the results from this work with the blue and orange stars, with the dashed blue line indicating the slope of the *Swift* matches and the orange dashed line the slope of the *NICER* detection matches. The *NICER* upper limit matches are the open orange stars. The BH population slope is indicated with the black dashed line and the upper limits from the MAXI J0911 and XTE J1701 observations are indicated with the cyan and black open circles, respectively.

3 RESULTS

3.1 SAX J1808

In the X-rays, our *NICER* results reveals the outburst of SAX J1808 to have a main outburst and subsequent reflaring (top panel of Fig. 1) within the 1–10.0 keV energy band. The main outburst rises around 2019 August 6 (MJD = 58701) and the reflaring around 2019 August 27 (MJD = 58722). The five detections we record here from *Swift* only display the decline of the main outburst with a peak flux at $(7.27 \pm 0.16) \times 10^{-10}$ erg s^{-1} cm^{-2} on the 2019 August 12 (MJD = 58708.47, second panel of Fig. 1). While our *NICER* results reveal a peak flux $(6.20 \pm 0.018) \times 10^{-10}$ erg s^{-1} cm^{-2} (247 counts s^{-1}, MJD = 58705.01 in the first panel of Fig. 1), similarly Bult et al. (2019) record a peak bolometric flux of $(4.7 \pm 0.5) \times 10^{-10}$ erg s^{-1} cm^{-2} within the 0.01–100 keV energy band. SAX J1808 was undetected in the first two epochs of the MeerKAT monitoring. These non-detections have upper limits of 0.075 and 0.12 mJy beam^{-1} at 3σ, respectively (indicated with upside-down triangles in the third panel of Fig. 1). The light curve was constructed using the flux measurements from PYBDSF such that the radio flare is seen to peak at 0.59 ± 0.034 mJy beam^{-1}. We observe a decline in the radio light curve between 10 and 23 August (MJD = 58705–58718) but the rise of a reflare event is seen between the 5th and 6th epoch (23–31 August, MJD = 58718–58726) as an increase from 0.11 to 0.16 mJy beam^{-1} is measured. In addition to the LCO optical data, the source was observed with MeerLICHT, a prototype of the BlackGEM array (Bloemen et al. 2016; Groot 2019) which provides simultaneous monitoring of the same area of the sky as MeerKAT. The data were processed automatically with the BLACKBOX/ZOGY pipeline (Vreeswijk & Paterson 2021), which performs primary reductions that include bias subtraction, overscan corrections and flat-fielding, as well as astrometric and photometric calibrations. Daily averages of each band were determined by co-adding the images and ranged between 17.89 ± 0.04 and 19.38 ± 0.06 mag across all bands. The results from MeerLICHT, which we do not plot, confirm the results from the more comprehensive data from LCO displayed in the bottom panel of Fig. 1.

3.2 MAXI J0911 and XTE J1701

In the radio, neither MAXI J0911 nor XTE J1701 were detected. The 3σ upper limits presented in Table 1 represent that of the single radio:X-ray matches for each source. Assuming a flat spectral index the radio flux was converted to a frequency of 5 GHz such that the luminosity νL_ν is $5L_5$ (referred to as radio luminosity L_R in the paper). The luminosity upper limits are $L_R < 3.57 \times 10^{28}$ erg s^{-1} and $L_R < 4.29 \times 10^{28}$ erg s^{-1} taken on MJD 59421.65 and 59421.76 respectively (2021 July 26) for MAXI J0911 and XTE J1701, respectively. These luminosities were determined using distances 10.4 kpc (Tudor et al. 2016) and 10 kpc (Fender et al. 2007) for MAXI J0911 and XTE J1701, respectively and the upper limits are plotted in cyan (MAXI J0911) and black open circles (XTE J1701) in Fig. 2.

4 DISCUSSION

In this section, we discuss the 2019 outburst of SAX J1808 and the placement of the sources (in this work) on the radio:X-ray correlation.

Table 1. The MeerKAT radio flux densities (1.28 GHz) and luminosities at 5 GHz, along with *Swift* and *NICER* X-ray flux and luminosities matches from the 1–10 keV energy band. The upper limits are 3σ and the uncertainties in the table are 1σ. The luminosities are based on distance estimates of 3.5, 10.4, and 10 kpc for SAX J1808, MAXI J0911, and XTE J1701, respectively. The *Swift* and *NICER* radio:X-ray matches are indicated as $S^{1,2,3}$ and $N_{1,2,3,4,5,6}$, respectively, next to the MJDs.

MJD	F_r (mJy beam^{-1})	$F_{xNICER} \times 10^{-10}$ (erg s^{-1} cm^{-2})	$F_{xSwift} \times 10^{-10}$ (erg s^{-1} cm^{-2})	$L_r \times 10^{28}$ (erg s^{-1})	$L_{xNICER} \times 10^{36}$ (erg s^{-1})	$L_{xSwift} \times 10^{36}$ (erg s^{-1})
SAX J1808						
58695.02_{N1}		0.0040 ± 0.0002			$0.000\,59 \pm 0.000\,03$	
58695.74_{N1}	<0.075			<0.56		
58699.27_{N2}		0.0060 ± 0.0002			$0.000\,88 \pm 0.000\,03$	
58699.82_{N2}	<0.12			<0.86		
58705.01_{N3}		6.20 ± 0.02			0.910 ± 0.003	
58705.81^{S1}_{N3}	0.59 ± 0.04			4.32 ± 0.25		
58708.47^{S1}			7.27 ± 0.16			$1.065^{+0.023}_{-0.024}$
58710.40			6.33 ± 0.16			0.930 ± 0.023
58711.05_{N4}		4.70 ± 0.01			0.700 ± 0.002	
58711.95^{S2}_{N4}	0.36 ± 0.02			2.67 ± 0.15		
58712.65^{S2}			3.98 ± 0.14			0.58 ± 0.02
58718.70_{N5}	0.11 ± 0.02			0.83 ± 0.15		
58719.00_{N5}		0.920 ± 0.005			0.1300 ± 0.0007	
58726.79^{S3}_{N6}	0.16 ± 0.02			1.20 ± 0.13		
58726.98_{N6}		0.80 ± 0.02			0.20 ± 0.02	
58728.45^{S3}			$1.390^{+0.063}_{-0.066}$			$0.2030^{+0.0092}_{-0.0096}$
58740.81			$0.937^{+0.078}_{-0.065}$			$0.137^{+0.012}_{-0.010}$
58741.79						
MAXI J0911						
59403.25	<0.055		<2.32	<3.57		<3
XTE J1701						
59421.75	<0.072		<2094	<4.29		<2500

We only provide single upper limits of MAXI J0911 and XTE J1701, but the 2019 outburst results significantly extend SAX J1808's X-ray luminosity range on the plane.

4.1 SAX J1808 2019 outburst

Our results show that the X-ray peak follows the radio peak where maximum flux density is recorded as 0.59 ± 0.034 mJy beam^{-1}, indicating jet action from 2019 August 10 (MJD 58705). The optical reports of the 2019 outburst recorded (see Baglio et al. 2020; Goodwin et al. 2020) observations from LCO and the *Southern African Large Telescope* (*SALT*). Goodwin et al. (2020) caught the rise of the outburst with a peak optical flux > 1.2 mJy around the 10 August and we present the Baglio et al. (2020) light curve in bottom panel of Fig. 1 where we note two rise and dips occurrences (around 2019 July 22 to 2019 August 3 corresponding to MJDs 58686–58698) before the peak of the main outburst is seen around 2019 August 11 (MJD 58706). The reflaring event started around the 2019 August 24 and while we only see the start of this reflare in our radio results (third panel Fig. 1), it shows the jets are still present as suggested in Baglio et al. (2020). In Goodwin et al. (2020), the X-ray peak was detected on 2019 August 14 (MJD 58709). These reports together with our results suggest the optical peaked first and the X-ray and radio outbursts peaked later. This result may be explained by an outside-in outburst (see Ioannou et al. 1999) starting from the outer edges of the disc. The early optical activity in the 2019 outburst is discussed in more detail in Goodwin et al. (2020), proposing scenarios that stem from mass-transfer variations and geometrical effects of the disc. The cadence of our radio observations was not high enough to quantify the outside-in outburst mechanism.

4.2 The radio:X-ray correlation of SAX J1808

Fig.1 illustrates the evolution of the radio (MeerKAT) and X-ray (*NICER*, *Swift*) outburst in the first three panels. A flat spectral index is assumed and the radio luminosity is determined similarly to MAXI J0911 and XTE J1701 mentioned in Section 3.2; in the case of SAX J1808 the luminosities are based on a distance of 3.5 kpc (Galloway & Cumming 2006). Based on the 10 quasi-simultaneous *Swift* observations, the source was only detected in six epochs. After inspection, three epochs were selected which were within $\Delta t \sim 2$ d of three of the radio observations (see matches $S^{1,2,3}$ in Table 1). The radio and X-ray luminosities from the selected MJDs, were used to determine SAX J1808's position on the radio:X-ray correlation plot. Since the *NICER* observations are taken at higher cadence, we were able to match the six radio observations within $\Delta t \sim 1$ d (see matches $N_{1,2,3,4,5,6}$ in Table 1). The radio:X-ray correlation is shown in Fig. 2 where the blue stars indicate the 2019 outburst results based on the *Swift* matches and the orange stars are the *NICER* matches for the six radio observations. The previous $L_R L_X$ measurements of the source are shown with the green stars. In this figure SAX J1808 lies among the AMXP class of sources which are indicated with the pink stars. This is an expected result for the source since it is the cornerstone of the AMXP class, and we note that these results have less scatter than the previous outbursts. The upper limits of the *NICER* matches extend to lower radio and X-ray luminosities, revealing how extensive the luminosity range of the source can get on the correlation plane. The PYTHON module, LINEAR REGRESSION, in the SKLEARN library was used to determine a best fit of the SAX J1808 2019 outburst, the data points were fed into the model and as a result produced slopes $\beta = 0.77 \pm 0.13$ and $\beta = 0.67 \pm 0.33$ for the detection matches (excluding upper limits) of *Swift* and *NICER*, respectively. We also fit all the *NICER* matches (including the upper limits) and

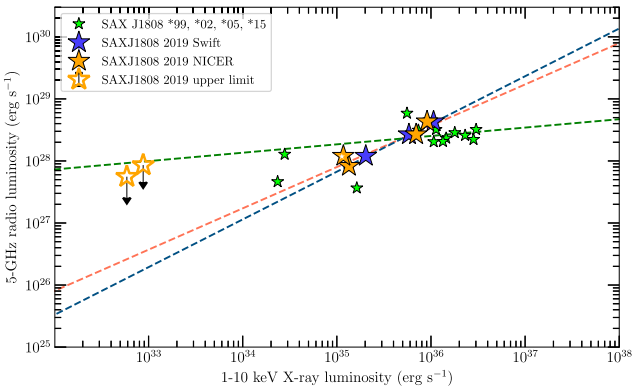

Figure 3. The radio:X-ray correlation slopes for the SAX J1808 outbursts; 2019 outburst (blue and orange), and a group of four of the older outbursts reported (green). The combination of all older outburst points on the figure (1999, 2002, 2005, and 2015) are fit to a slope of $\beta = 0.33 \pm 0.23$ and indicated with the green dashed line. The blue and orange dashed lines represent the detection matches (excluding upper limits) with slopes $\beta = 0.77 \pm 0.13$ and $\beta = 0.67 \pm 0.33$ for the *Swift* and *NICER* 2019 outburst, respectively. The NICER radio upper limit matches are presented as open orange stars.

the best-fitting slope was $\beta = 0.35 \pm 0.38$. The older outbursts results produced a fit of ($\beta = 0.33 \pm 0.23$), the combination of complete SAX J1808 points ($\beta = 0.34 \pm 0.20$) and the complete AMXP class ($\beta = 0.38 \pm 0.23$) only included the set of *Swift* matches (Fig. 3). These less steep slopes are suspected to be due to the increase in scatter of the overall sample of points of the source. The slope which includes the low luminosity upper limits from *NICER* is small too but with larger error, in contrast a recent report on intermittent AMXP Aql X-1 at low X-ray luminosities finds a slope of $\beta = 1.17^{+0.30}_{-0.21}$ where detection and upper limits of multiple outbursts are included for the fit (see more details in Gusinskaia et al. 2020). Gusinskaia et al. (2020) also fit detections only, these slopes (based on different hardness ratios) ranged between $\beta \sim 0.73$–0.96. This indicates that a single NS-XRB can have a varying slope depending on the outburst and the detections included in the fit. Furthermore, the radio:X-ray correlation for BHXBs and NS-XRBs from Coriat et al. (2011) reports the radiatively inefficient and efficient branches have slopes $\beta \sim 0.7$ and $\beta \sim 1.4$ for the BHXBs and NS-XRBs respectively. Similarly seen in Migliari et al. (2003), while some NS-XRB systems follow this trend, the slopes of SAX J1808 in this work match more closely to that of the BHXBs. This is a result that has been observed before for NS-XRBs. Tudor et al. (2017) demonstrated that the slope of AMXP IGR J00291 + 5934 is 0.77 ± 0.18, hence it does appear the correlation slopes of some NSs behave differently.

4.3 MAXI J0911−655

MAXI J0911, which resides in the globular cluster NGC 2808, was first detected with MAXI/GSC's (MAXI Gas Slit Camera) nova alert system in February 2016 (Mihara et al. 2011; Serino et al. 2016). The X-ray activity from the source was detected about a week later with *Swift*/BAT (Sanna et al. 2017). Later detections of X-ray activity prompted simultaneous radio follow-up with ATCA (Tudor et al. 2016), yielding an upper limit $L_R < 4.5 \times 10^{28}$ erg s^{-1} at 5 GHz. Assuming a flat spectrum and distance 10.4 kpc, we derive a 3σ upper limit $L_R < 3.57 \times 10^{28}$ erg s^{-1} based on MeerKAT observations taken in July 2021 (see cyan open circle in Fig. 2) after weak hard X-rays were detected in Ng et al. (2021).

4.4 XTE J1701

XTE J1701 is an important source in the study of NS-XRBs as it exhibited behavior associated with both 'Z' and 'Atoll'-type binaries, establishing that these classifications depend upon accretion state (Lin, Remillard & Homan 2009). Fender et al. (2007) reported a small number of radio detections of XTE J1701, which were broadly consistent with those reported for other Z-sources. They also reported an extended structure (labelled sources B, C, and D in fig. 5 of Fender et al. 2007) approximately 3 arcmin to the south which they speculated could be a large-scale jet associated with the outburst of the binary. This structure is visible in our MeerKAT image at flux densities consistent with being constant over ∼15 yr [see luminosity upper limits at 10 kpc (Fender et al. 2007) in Table 1 and spectral indexes Table 2, while the source is placed as the black open circle on the radio:X-ray plane in Fig. 2]. We therefore rule out any association with a transient jet associated with the binary, and attribute these sources to background extragalactic sources instead. The limit on the core radio luminosity from XTE J1701 is not particularly constraining given the quiescent state during the July 2021 observation.

5 CONCLUSION

NS-XRBs are an interesting class to study the disc/jet coupling since the radio:X-ray correlation tends to vary considerably in different sources and accretion regimes. We report here on the 2019 outburst of SAX J1808 as well as follow up observations of MAXI J0911 and XTE J1701 carried out as part of the ThunderKAT Large Survey Programme on MeerKAT (Fender et al. 2016). SAX J1808 is reported in the radio, X-ray, and the optical from MeerKAT, *Swift*, *NICER*, and LCO, respectively. The outburst lasted from July to early October 2019, including a main outburst event and a reflare event which started late August to early September 2019. These results suggest the peak of the main outburst is seen in the optical before the X-ray and radio which may imply an outside-in outburst (Ioannou et al. 1999), however, our radio observations were not sampled at a high enough cadence to suggest the mechanism occurred in this

Table 2. The peak flux density of the extended sources B, C, and D of XTE J1701 as indicated in fig. 5 of Fender et al. (2007), along with the spectral index between the MeerKAT (1.28 GHz) 2021 observation and the ATCA (4.8 and 8.6 GHz) 2006 observations in Fender et al. (2007).

Source	$F_{1.28}$ (mJy beam^{-1})	$F_{4.8}$ (mJy beam^{-1})	$F_{8.6}$ (mJy beam^{-1})	α (4.8–8.6)	α (1.28–4.8–8.6)
B	22.23	2.5	0.9	−1.7	−1.7
C	16.38	2.0	0.5	−2.4	−1.7
D	16.55	1.5	0.3	−2.7	−1.9

system. Furthermore, the reflaring event was associated with a radio re-brightening, indicating a strengthening of the jet in this phase (Baglio et al. 2020). The radio:X-ray correlation of the source in this work (*Swift* and *NICER* detection matches have a slope of $\beta \sim 0.77 \pm 0.13$ and $\beta \sim 0.67 \pm 0.33$, respectively) suggests a similar radiative efficiency compared to the BHXB standard slope of $\beta \sim 0.6$ (Corbel et al. 2000, 2003, 2013; Carotenuto et al. 2021). Finally, the upper limits of MAXI J0911 and XTE J1701 from both MeerKAT and *Swift* place the sources in their respective classes (AMXP the former, Z/Atoll the latter). And while these are non-detections the results encourage continued monitoring of these sources and similar NS-XRBs to improve our understanding and reveal the true nature of the disc and jet coupling in XRBs.

ACKNOWLEDGEMENTS

KVSG, IMM, PAW, and PJG acknowledge support from the University of Cape Town and the National Research Foundation. KVSG would like to thank Dave Russell for making the LCO data published in Baglio et al. (2020) available for the improvement of this paper. KVSG acknowledges Lauren Rhodes for the advice during radio data processing. PJG is supported by NRF SARChI grant no. 111692. SEM acknowledges financial contribution from the agreement ASI-INAF no. 2017-14-H.0, and PRIN-INAF 2019 no. 15. DRAW was supported by the Oxford Centre for Astrophysical Surveys, which is funded through generous support from the Hintze Family Charitable Foundation. JvdE is supported by a Lee Hysan Junior Research Fellowship awarded by St. Hilda's College, Oxford. IH acknowledges support from the UK Science and Technology Facilities Council (ST/N000919/1) and from the South African Radio Astronomy Observatory. VAM acknowledges support from the National Research Foundation grant no. 119466.

The MeerKAT telescope is operated by the South African Radio Astronomy Observatory, which is a facility of the National Research Foundation, an agency of the Department of Science and Innovation. We acknowledge the use of public data from the *Swift*/BAT/*XRT* data archive. We acknowledge the use of the ilifu cloud computing facility – www.ilifu.ac.za, a partnership between the University of Cape Town, the University of the Western Cape, the University of Stellenbosch, Sol Plaatje University, the Cape Peninsula University of Technology, and the South African Radio Astronomy Observatory. The Ilifu facility is supported by contributions from the Inter-University Institute for Data Intensive Astronomy (IDIA – a partnership between the University of Cape Town, the University of Pretoria, the University of the Western Cape, and the South African Radio astronomy Observatory), the Computational Biology division at UCT and the Data Intensive Research Initiative of South Africa (DIRISA).

DATA AVAILABILITY

The data underlying this article will be shared on reasonable request to the corresponding author.

REFERENCES

Alpar M. A., Cheng A. F., Ruderman M. A., Shaham J., 1982, Nature, 300, 728
Backer D. C., Kulkarni S. R., Heiles C., Davis M. M., Goss W. M., 1982, Nature, 300, 615
Baglio M. C. et al., 2020, ApJ, 905, 87
Bahramian A. et al., 2018, Radio/X-ray correlation database for X-ray binaries
Bloemen S. et al., 2016, in Hall H. J., Gilmozzi R., Marshall H. K.eds, Proc. SPIE Conf. Ser. Vol. 9906, Ground-based and Airborne Telescopes VI. SPIE, Bellingham, p. 990664
Bult P. et al., 2019, ApJ, 885, L1
Burrows D. N. et al., 2005, Space Sci. Rev., 120, 165
Carotenuto F. et al., 2021, MNRAS, 505, L58
Chakrabarty D., Morgan E. H., 1998, Nature, 394, 346
Corbel S., Fender R. P., Tzioumis A. K., Nowak M., McIntyre V., Durouchoux P., Sood R., 2000, A&A, 359, 251
Corbel S., Nowak M. A., Fender R. P., Tzioumis A. K., Markoff S., 2003, A&A, 400, 1007
Corbel S., Coriat M., Brocksopp C., Tzioumis A. K., Fender R. P., Tomsick J. A., Buxton M. M., Bailyn C. D., 2013, MNRAS, 428, 2500
Coriat M. et al., 2011, in Romero G. E., Sunyaev R. A., Belloni T.eds, Proc. IAU Symp. 275, Jets at All Scales. Cambridge Univ. Press, Cambridge, p. 255
Deller A. T. et al., 2015, ApJ, 809, 13
Fender R., Belloni T., 2012, Science, 337, 540
Fender R. P., Kuulkers E., 2001, MNRAS, 324, 923
Fender R. P., Dahlem M., Homan J., Corbel S., Sault R., Belloni T. M., 2007, MNRAS, 380, L25
Fender R. et al., 2016, Proc Sci., MeerKAT Science: On the Pathway to the SKA. Sissa, Trieste, PoS#13
Gallo E., Fender R. P., Pooley G. G., 2003, MNRAS, 344, 60
Gallo E., Degenaar N., van den Eijnden J., 2018, MNRAS, 478, L132
Galloway D. K., Cumming A., 2006, ApJ, 652, 559
Gendreau K. C., Arzoumanian Z., Okajima T., 2012, in Takahashi T., Murray S. S., den Herder J.-W. A.eds, Proc. SPIE Conf. Ser. Vol. 8443, Space Telescopes and Instrumentation 2012: Ultraviolet to Gamma Ray. SPIE, Bellingham, p. 844313
Goodwin A. J. et al., 2020, MNRAS, 498, 3429
Groot P. J., 2019, Nature Astron., 3, 1160
Gusinskaia N. V. et al., 2020, MNRAS, 492, 2858
Hasinger G., van der Klis M., 1989, A&A, 225, 79
Heywood I., 2020, Astrophysics Source Code Library, record ascl:2009.003
Homan J. et al., 2007, ApJ, 656, 420
Homan J., Sivakoff G., Pooley D., Heinke C., Strader J., Tudor V., Miller-Jones J., 2016, The Astron. Telegram, 8971, 1
in't Zand J. J. M., Heise J., Muller J. M., Bazzano A., Cocchi M., Natalucci L., Ubertini P., 1998, A&A, 331, L25
Ioannou Z., Naylor T., Welsh W. F., Catalán M. S., Worraker W. J., James N. D., 1999, MNRAS, 310, 398
Jahoda K., Markwardt C. B., Radeva Y., Rots A. H., Stark M. J., Swank J. H., Strohmayer T. E., Zhang W., 2006, ApJS, 163, 401
Joss P. C., Avni Y., Rappaport S., 1978, ApJ, 221, 645
Levine A. M., Bradt H., Cui W., Jernigan J. G., Morgan E. H., Remillard R., Shirey R. E., Smith D. A., 1996, ApJ, 469, L33
Lin D., Remillard R. A., Homan J., 2009, ApJ, 696, 1257
McMullin J. P., Waters B., Schiebel D., Young W., Golap K., 2007, in Shaw R. A., Hill F., Bell D. J.eds, ASP Conf. Ser. Vol. 376, Astronomical Data Analysis Software and Systems XVI. Astron. Soc. Pac., San Francisco, p. 127
Migliari S., Fender R. P., 2006, MNRAS, 366, 79
Migliari S., Fender R. P., Rupen M., Jonker P. G., Klein-Wolt M., Hjellming R. M., van der Klis M., 2003, MNRAS, 342, L67
Mihara T. et al., 2011, PASJ, 63, S623
Mohan N., Rafferty D., 2015, Astrophysics Source Code Library, record ascl:1502.007
Moin A., Reynolds C., Miller-Jones J. C. A., Tingay S. J., Phillips C. J., Tzioumis A. K., Nicolson G. D., Fender R. P., 2011, MNRAS, 414, 3551
Muno M. P., Remillard R. A., Chakrabarty D., 2002, ApJ, 568, L35
Ng M., Bult P. M., Strohmayer T. E., Sanna A., Gendreau K. C., Ho W. C. G., Arzoumanian Z., 2021, The Astron. Telegram, 14767, 1
Offringa A. R. et al., 2014, MNRAS, 444, 606
Patruno A., Watts A. L., 2021, in Belloni T. M., Méndez M., Zhang C.eds, Astrophysics and Space Science Library, Vol. 461, Timing Neutron Stars: Pulsations, Oscillations and Explosions. Springer, Berlin, p. 143
Sanna A. et al., 2017, A&A, 598, A34

Serino M. et al., 2016, The Astron. Telegram, 8872, 1
Srinivasan G., 2010, New A Rev., 54, 93
Tudor V. et al., 2016, The Astron. Telegram, 8914, 1
Tudor V. et al., 2017, MNRAS, 470, 324
Tudose V., Fender R. P., Linares M., Maitra D., van der Klis M., 2009, MNRAS, 400, 2111
van den Eijnden J. et al., 2021, MNRAS, 507, 3899
Verner D. A., Ferland G. J., Korista K. T., Yakovlev D. G., 1996, ApJ, 465, 487
Vreeswijk P., Paterson K., 2021, Astrophysics Source Code Library, record ascl:2105.011
Wijnands R., van der Klis M., 1998, ApJ, 507, L63
Williams D., Motta S., Fender R., Woudt P., Miller-Jones J., 2019, Astron. Telegram, 13026, 1
Wilms J., Allen A., McCray R., 2000, ApJ, 542, 914

This paper has been typeset from a TEX/LATEX file prepared by the author.